Nonideal mixing of phosphatidylserine and phosphatidylcholine in the fluid lamellar phase

Juyang Huang, Joy E. Swanson, Andrew R. G. Dibble, Anne K. Hinderliter, and Gerald W. Feigenson
Section of Biochemistry, Molecular and Cell Biology, Cornell University, Ithaca, New York 14853 USA

ABSTRACT The mixing of phosphatidylserine (PS) and phosphatidylcholine (PC) in fluid bilayer model membranes was studied by measuring binding of aqueous Ca^{2+} ions. The measured $[Ca^{2+}]_{aq}$ was used to derive the activity coefficient for PS, γ_{PS}, in the lipid mixture. For (16:0, 18:1)PS in binary mixtures with either (16:0, 18:1)PC, (14:1, 14:1)PC, or (18:1, 18:1)PC, $\gamma_{PS} > 1$; i.e., mixing is nonideal, with PS and PC clustered rather than randomly distributed, despite the electrostatic repulsion between PS headgroups. To understand better this mixing behavior, Monte Carlo simulations of the PS/PC distributions were performed, using Kawasaki relaxation. The excess energy was divided into an electrostatic term U^{el} and one adjustable term including all other nonideal energy contributions, ΔE_m. U^{el} was calculated using a discrete charge theory. Kirkwood's coupling parameter method was used to calculate the excess free energy of mixing, ΔG^E_{mix}, hence ln $\gamma_{PS,calc}$. The values of ln $\gamma_{PS,exp}$ and ln $\gamma_{PS,calc}$ were equalized by adjusting ΔE_m in order to find the simulated PS/PC distribution that corresponded to the experimental results. We were thus able to compare the smeared charge calculation of $[Ca^{2+}]_{surf}$ with a calculation ("masked evaluation method") that recognized clustering of the negatively charged PS: clustering was found to have a modest effect on $[Ca^{2+}]_{surf}$, relative to the smeared charge model. Even though both PS and PC tend to cluster, the long-range nature of the electrostatic repulsion reduces the extent of PS clustering at low PS mole fraction compared to PC clustering at an equivalent low PC mole fraction.

INTRODUCTION

The possibility of non-random mixing of lipids in biomembranes has widespread implications for cell biology, including possible formation of recognition sites and localized protein microenvironments (1) and modulation of chemical reactions of biomembrane constituents (2). Many different physical techniques have indicated nonrandom mixing in biomembranes, persisting on a variety of timescales and sizescales (3–5). The underlying basis for the heterogeneity has been suggested to be cytoskeletal interaction, focal gain or loss of membrane, or nearest-neighbor dependence of the free energy of mixing (2).

In chemically simple mixtures of lipids used as models for biomembranes the free energy of mixing can be isolated from other effects. Indeed, it has been clear for many years from the phase diagrams of simple lipid mixtures that lipids with different headgroups or acyl chains mix non-randomly (6, 7). A proper way to characterize this non-randomness, or nonideality, is to find the thermodynamic activity of the lipids in the mixture. The thermodynamic activity provides predictive power for the behavior of the molecule. Unfortunately, the thermodynamic activity is difficult to determine, even in simple binary mixtures in a chemically well-defined bilayer model membrane. A method that has been used is to simulate the shape of the liquidus and solidus boundaries of a binary lipid phase diagram (8). The principal constraints here are the experimental limitation to lipid pairs, both having gel-fluid transitions well above 0°C, and the conceptual limitation of analysis using, for example, regular solution theory or quasichemical approximation. The experimental limitation is quite important because most natural phospholipids have a gel-fluid transition well below 0°C. The conceptual limitations are problematic, since in general, two adjustable parameters are needed to fit the phase diagram data (8–10). A promising development is the use of order parameters of spin-labeled lipids in mixtures to estimate the activity coefficients (11).

In this study, we use an indirect method to measure the thermodynamic activity of phosphatidylserine, PS, in the fluid bilayer. This method is of a general type in which the membrane-bound molecule reacts with ions in the electrical double layer (12). An example of this type of method would be H^+ ion binding to a membrane-bound base, with the stoichiometric chemical binding reaction, $H^+ + A^- \rightleftharpoons HA$, detected by perhaps NMR, EPR, absorption, or fluorescence spectroscopy, or bulk pH, as appropriate (12–14). In this study, the ion is Ca^{2+} and the stoichiometric chemical reaction, $Ca^{2+} + 2PS^- \rightleftharpoons Ca(PS)_2$, is detected by measuring high-affinity Ca^{2+} binding. This reaction has been characterized in previous studies (15, 16). A key finding was that in fluid mixtures of phosphatidylserine and phosphatidylcholine (PS/PC) only the PS reacts with Ca^{2+}, i.e., no PC could be detected in the product $Ca(PS)_2$. The aqueous Ca^{2+} concentration, $[Ca^{2+}]_{aq}$, is then related to the thermodynamic activity of PS, $\mathbf{a}_{PS}$, in the fluid PS/PC mixture. However, the earlier analyses erred in equating $\mathbf{a}_{Ca^{2+},aq}$ with the activity of Ca^{2+} near the bilayer surface, $\mathbf{a}_{Ca^{2+},surf}$. A simple form of correction is to measure or calculate the smeared charge surface potential Ψ, then calculate

Address correspondence to Dr. Gerald W. Feigenson, Section of Biochemistry, 201 Biotechnology Building, Cornell University, Ithaca, NY 14853, USA.

$$[Ca^{2+}]_{surf} = [Ca^{2+}]_{aq} \exp(-2e\Psi/kT), \quad (1)$$

where e is the magnitude of the electronic charge, k is the Boltzmann constant, and T is the absolute temperature. We describe the results of data analysis using this correction, together with a new version of the calculation of surface ion concentration, which describes the local ion concentration for the case where membrane-bound charge is not smeared over the surface, but is instead clustered. This new method involves computer simulation of the 2-dimensional distribution of PS and PC in the bilayer mixture. We describe how to find the calculated distribution of PS and PC that agrees with the experimentally determined PS activity coefficient.

MATERIALS AND METHODS

Materials

1-palmitoyl-2-oleoyl-*sn*-glycero-3-phosphoserine ((16:0, 18:1)PS), 1-palmitoyl-2-oleoyl-*sn*-glycero-3-phosphocholine ((16:0, 18:1)PC), 1,2-dimyristoleoyl-*sn*-glycero-3-phosphocholine ((14:1, 14:1)PC), and 1,2-dioleoyl-*sn*-glycero-3-phosphocholine ((18:1, 18:1)PC) from Avanti Polar Lipids, Inc. (Birmingham, AL), showed no impurities when 50 μg was chromatographed on Adsorbosil plus P TLC plates with chloroform/methanol/concentrated NH_3, 25/10/2 vol/vol or chloroform/methanol/water, 65/25/4, vol/vol; the calcium chelator/indicators 1,2-bis(*o*-aminophenoxy)ethane-N,N,N′,N′-tetraacetic acid (BAPTA) and 1,2-bis(*o*-amino-5-bromophenoxy)ethane-N,N,N′,N′-tetraacetic acid (BrBAPTA) were from Molecular Probes (Junction City, OR); piperazine-N,N′-bis(2-ethanesulfonic acid) (Pipes), purest grade, was from A. G. Fluka Corp. (Hauppauge, NY). Calcium carbonate, ultrex grade, and the phosphate standard, analytical grade, were from J. T. Baker, Inc. (Bricktown, NJ). Chelex-100 ion-exchange resin was from Bio-Rad Labs (Rockville Center, NY). Water was purified through a Milli-Q water purifying system. All other chemicals were of reagent grade.

Measurement of Ca^{2+} binding

The preparation of samples was essentially as described by Swanson and Feigenson (16), except that the removal of contaminating Ca^{2+} from the buffer (20 mM Pipes, 100 mM KCl, pH 7.00) was effected by passing the buffer through a column of Chelex, rather than by batchwise equilibration with Chelex.

Multilamellar dispersions of PS/PC were prepared from lipid mixtures that had been lyophilized from benzene/methanol, 19/1 vol/vol, and $[Ca^{2+}]_{aq}$ was measured using the Ca^{2+} chelator/indicators BAPTA and BrBAPTA, as described (16). Briefly, the first part of the procedure is to allow Ca^{2+} binding to the extent of about 5–10% of the total quantity of PS, with $[Ca^{2+}]_{aq}$ controlled at about 5–10× the equilibrium value by use of Ca^{2+} chelator. The next step is to dissolve about 10% of the $Ca(PS)_2$ that had formed during the binding period, by adding a small quantity of BAPTA or BrBAPTA. The final step is to measure the $[Ca^{2+}]_{aq}$ by determining the chelator spectrum. The dissolving step is repeated until $[Ca^{2+}]_{aq}$ no longer changes. The entire procedure, which takes about one month, results in equilibration of the three phases in the system, i.e., $[Ca^{2+}]_{aq}$, fluid PS/PC, and $Ca(PS)_2$.

The experimental objective is to find the activity coefficient γ_{PS}, in the fluid bilayer mixture of PS/PC. The measured value of $[Ca^{2+}]_{aq}$ is used to find the concentration of Ca^{2+}, $[Ca^{2+}]_{surf}$, that reacts with the PS, by use of Eq. 1 or else as described below. With a standard state of $\gamma_{PS} = 1$ for mole fraction $\chi_{PS} = 1$, the definition $\mathbf{a}_{PS} = \gamma_{PS}\chi_{PS}$, and following Feigenson (15):

$$\gamma_{PS} = \{[Ca^{2+}]_{surf,at\ \chi_{PS}=1}/[Ca^{2+}]_{surf,at\ \chi_{PS}}\}^{1/2}/\chi_{PS}. \quad (2)$$

Lattice model for computer simulations

We model the PS/PC membrane as a 2-dimensional triangular lattice. Each lattice site can be occupied by either a PS or a PC lipid. The area of each site is 62 $Å^2$ (17). The total number of lipids (N), the number of PS (N_{PS}), and the number of PC (N_{PC}), are fixed for each simulation.

The total energy U^T of the PS/PC lattice is divided into four terms, with the strategy of explicitly placing the long-range electrostatic repulsion energy between PS molecules into one term $U^{el}(\chi_{PS})$, and then accounting for all other (shorter range) interactions as nearest-neighbor contributions:

$$U^T = N_{PS\text{-}PS}U_{PS\text{-}PS} + N_{PC\text{-}PC}U_{PC\text{-}PC} + N_{PS\text{-}PC}U_{PS\text{-}PC} + U^{el}(\chi_{PS}), \quad (3)$$

where $U_{PS\text{-}PS}$, $U_{PC\text{-}PC}$, and $U_{PS\text{-}PC}$ are the interaction energies for the designated lipid contacts, and $N_{PS\text{-}PS}$, $N_{PC\text{-}PC}$, and $N_{PS\text{-}PC}$ are the total number of the designated lipid contacts in the lattice. $U^{el}(\chi_{PS})$ is the electrostatic energy (treated in detail below) of PS at PS mole fraction χ_{PS}. For this lattice system, one can show that

$$Z N_{PS} = 2N_{PS\text{-}PS} + N_{PS\text{-}PC},$$

and

$$Z N_{PC} = 2N_{PC\text{-}PC} + N_{PS\text{-}PC},$$

where Z is the number of nearest neighbors to a lattice site, which is 6 for a triangular lattice. U^T can now be rewritten as:

$$U^T = ZN_{PS}U_{PS\text{-}PS}/2 + Z N_{PC}U_{PC\text{-}PC}/2 + N_{PS\text{-}PC}[U_{PS\text{-}PC} - (U_{PS\text{-}PS} + U_{PC\text{-}PC})/2] + U^{el}(\chi_{PS}).$$

We define the non-electrostatic excess mixing energy of PS and PC, ΔE_m, as (18)

$$\Delta E_m = U_{PS\text{-}PC} - (U_{PS\text{-}PS} + U_{PC\text{-}PC})/2. \quad (4)$$

The total energy of a PS/PC mixture is then given by:

$$U^T = ZN_{PS}U_{PS\text{-}PS}/2 + Z N_{PC}U_{PC\text{-}PC}/2 + N_{PS\text{-}PC}\Delta E_m + U^{el}(\chi_{PS}). \quad (5)$$

The first two terms of U^T are constants, therefore they do not contribute to the nonideal mixing of two lipids. For the purpose of canonical Monte Carlo simulation, only the last two terms are used.

The mixing behavior of PS and PC is governed by the two interaction energy terms in Eq. 5. If ΔE_m is positive it tabulates an energy cost for forming PS–PC neighbors: like molecules will tend to form clusters, thereby reducing the number of PS–PC contacts. If ΔE_m is negative, the situation is opposite: the two types of lipids tend to mix uniformly to increase PS–PC contacts. On the other hand, the electrostatic repulsion U^{el} between PS molecules will always make an unfavorable contribution to PS–PS contacts. With the presence of both electrostatic repulsion and a positive ΔE_m, there would be competition between these two energy terms. When ΔE_m is large enough, the electrostatic repulsion will be overcome, and clusters of PS and of PC will form.

Calculation of electrostatic energy

Although membrane electrostatic potential plays an essential role in a variety of biomembrane phenomena, current understanding is still

quite deficient. Some of the problems are: (*a*) choice of the dielectric constant within the membrane; (*b*) extent of the region of chosen dielectric constant; (*c*) location of the charges within a region, including time dependence of this charge location; and (*d*) magnitude of the (partial) charge. To get a reasonable estimate of the electrostatic interaction of charged lipid head groups is thus a difficult task.

First we need to choose a model of membrane electrostatics to calculate the electrostatic interaction of PS headgroups within the membrane. We do not require a smeared charge treatment, since we use computer simulation to study the nonideal mixing of the lipids. Furthermore, we want to study lipid mixtures at various PS mole fractions, including the pure PS case wherein the surface potential is high. Most discrete charge theories (19–21) are not applicable at high χ_{PS}, because they use a linearized form of the Poisson–Boltzmann equation, which is valid only at low surface potential ($\Psi \leq 25$ mV).

For our simulation, we used a discrete charge theory developed by Sauvé and Ohki (22). The theory is based on the linearization of the Poisson–Boltzmann equation around a "smeared surface charge" solution. The Hankel transform technique is then used to solve the linear equations. The same technique was earlier used to study the adsorption of ions at the metal-water interface by Loeb (23) and Levine et al. (24), and later used by Duniec and Thorne to calculate the electrostatic potential profiles across a lipid bilayer membrane for a given charge distribution (25, 26). In this discrete charge membrane potential theory, the membrane plus electrolyte is modeled to have three regions: (*a*) a non-polar region, of dielectric constant ϵ_m, that contains no charge and consists of hydrocarbon chains; (*b*) an adsorption or polar region, of dielectric constant ϵ, in which the polar head groups and fixed charges are located; and (*c*) an aqueous phase, of dielectric constant ϵ_0, which contains the electrical double layer. With this theory, the local electrostatic potential produced by an arbitrary arrangement of charged particles within the polar region can be calculated. One advantage of this theory is that it can be used to calculate the non-uniform surface potential arising from the charged particle distribution, while also giving an average surface potential which is the same as that from a smeared charge model.

We choose $\epsilon_m = 3$, $\epsilon = 30$, and $\epsilon_0 = 78$ (27, 28). The thickness of the $\epsilon = 30$ region is taken as 8 Å. We approximate the two negative charges and single positive charge of the PS headgroup as a single (fractional) point charge located at the midplane of the $\epsilon = 30$ region. The binding of K^+ within the potential-determining region (as distinguished from K^+ binding within the electrical double layer) is treated as reducing the PS negative charge to a fractional value.[1] The overall extent of this K^+ binding is determined from Gouy–Chapman–Stern treatment, using the binding constant to *fluid* phase PS for Ca^{2+} of 12 M^{-1} (29) and for K^+ of 0.4 M^{-1}. The latter value was calculated from the measured zeta potential of −59 mV for pure (16:0, 18:1)PS vesicles in our buffer of 100 mM KCl, 20 mM Pipes, pH 7.00 (McLaughlin, S., personal communication).

We thus define the partial charge on each PS as

$$p = (N_{K^+\text{bound}} - N_{PS})/N_{PS}. \tag{6}$$

In the polar region, the electrostatic potential (Ψ^{PS}) at each PS can be expressed as two parts (22):

$$\Psi^{PS} = \Psi_{const} + \Psi_{add}, \tag{7}$$

where Ψ_{const} is the constant part of the potential, which is independent of the lateral distribution of PS; Ψ_{add} is the additive part of the potential, which is dependent on the local environment of the particular PS lattice site. The term Ψ_{const} contains the contribution from the ions in the double layer, together with the image charge of this particular PS molecule. The term Ψ_{add} contains the contribution from all other PS and their image charges. This potential is pairwise additive.

Unlike more recent electrostatic theories (30, 31), the discrete charge theory of Sauvé and Ohki neglects all inter-ionic correlation effects of the electrolyte. This will lead to serious error in estimating the membrane surface potential and ion concentration profile near the membrane for multivalent electrolyte or at high electrolyte concentration (30, 32). However, for the experimental conditions of our Ca^{2+} binding measurements (0.1 M KCl), Monte Carlo simulations show the error is rather small (33, 34).

The electrostatic energy of a PS/PC mixture is given by

$$U^{el}(\chi_{PS}) = epN_{PS}\psi_{const} + \sum_{i=1}^{N_{PS}} ep\psi^i_{add}/2, \tag{8}$$

where the summation is carried over all the PS molecules. The formulation of Eq. 8 is based on the interpretation of Eq. 7: i.e., the electrostatic potential experienced by a particular PS is composed of a constant component Ψ_{const} and a distribution-dependent sum from other PS, Ψ_{add}. The first part of the right side of the Eq. 8 represents the energy of all PS in a constant external field, Ψ_{const}, and the second part is the energy that is analogous to the energy of a point charge particle system (35).

Simulation of lipid lateral distribution

All the simulations were performed on a 100 × 100 triangular lattice with standard periodical boundary conditions. For each simulation, χ_{PS}, ΔE_m, and T were held constant (i.e., a canonical ensemble). The Kawasaki relaxation method (36) was used to bring the system to equilibrium: a lipid can interchange its position with that of a nearest neighbor with a probability proportional to $\exp(-\Delta U)$, where ΔU is the energy difference of the system due to the interchange (termed a "lipid move"). A detailed illustration of the Kawasaki relaxation method can be found in Jan et al. (37). In addition to the nearest neighbor interaction, the long-range electrostatic interaction of PS head groups is also taken into account. Thus, for each lipid move, the electrostatic contribution from 104 nearest lattice sites is calculated, i.e., within a radius of about 5 lipid diameters. Contribution from sites farther away was not calculated, because these make only a very small contribution to the energy difference of the move, and also will be thermally averaged in real membranes. In each simulation, the ensemble average of the energy of the mixture and of the number of PS molecules surrounding each PS were obtained in 500 Monte Carlo steps *after* the system had reached equilibrium. Equilibrium was determined by the convergence of the energies of mixtures started from different initial states. Initial states ranged from randomly mixed (high temperature) to completely segregated blocks of PS and PC.

[1] Each PS can be treated as having a partial negative charge if two conditions are met: (1) K^+ binds to PS in the potential-determining layer. This ion, as well as other mono and divalent cations, appears to have a true, chemical binding to PS, in addition to accumulation in the electrical double layer, as determined by measurements of ion binding and vesicle electrophoretic mobility (45, 46). (2) Each PS in the lattice experiences K^+ binding and dissociation events before a change in lattice position. We estimate that K^+ associates with a PS site $\sim 2 \times 10^7\ s^{-1}$ (i.e., the rate of association is dependent upon $[K^+]_{surf}$; for χ_{PS} ranging from 0.2 to 1.0, $[K^+]_{surf}$ varies from ~0.3 to 1 M in our buffer, and thus $k_{on} \times [K^+]_{surf}$ ranges from ~1 to $3 \times 10^7\ s^{-1}$) and dissociates approximately $10^8\ s^{-1}$, whereas a PS exchanges with a neighboring site on the lattice only about 10^6–$10^7\ s^{-1}$ (47). The association and dissociation rates are based on a K^+–PS association constant of 0.4 M^{-1}, together with the Co^{2+}–PS association constant of about 30 M^{-1} and dissociation rate constant of $10^6\ s^{-1}$, determined by McLaughlin (48). We assume that Co^{2+} and K^+ association rate constants for PS in the bilayer are similar, and the difference in the measured equilibrium association constants reflects only differences in the lifetimes of the two different ion complexes with PS.

Calculation of excess Gibbs free energy

To calculate excess Gibbs free energy of a lipid mixture by computer simulation, we used Kirkwood's coupling parameter method (38–40). The advantages of the coupling parameter method are that the quantities to be determined in the simulation are statistically well behaved, and also that a low particle density condition is not required, as in the test particle method (41).

The molar excess Gibbs free energy of a binary mixture at fixed temperature T and fixed pressure P can be written as (38)

$$\Delta G^{E}_{mix} = \chi_{PS}(g^{res}_{mix} - g^{res}_{pure\ PS}) + \chi_{PC}(g^{res}_{mix} - g^{res}_{pure\ PC}). \quad (9)$$

Where the residual free energies are defined by

$$g^{res}_{mix} = g_{mix} - g_{ig},$$

with g_{ig} the Gibbs free energy of an ideal gas mixture at the same temperature, pressure, and composition. Since $\chi_{PS} + \chi_{PC} = 1$, Eq. 9 can also be written as

$$\Delta G^{E}_{mix} = g^{res}_{mix} - g^{res}_{pure\ PC} - \chi_{PS}(g^{res}_{pure\ PS} - g^{res}_{pure\ PC}). \quad (10)$$

Applying Kirkwood's coupling parameter method (38) to our lattice model of the PS/PC lipid mixture, the molar excess Gibbs free energy of a PS/PC mixture is given by (see Appendix for details):

$$\Delta G^{E}_{mix} = N_o\left\{\left[\int_0^1 \langle U^{el}(\chi_{PS})\rangle\Big|_{\lambda_E=0} d\lambda_\psi - \chi_{PS}U^{el}(\chi_{PS}=1)\right]\Big/N + \int_0^{\Delta E_m} \langle N_{PS\text{-}PC}\rangle\Big|_{\lambda_\psi=1} \Big/ N\, d\lambda_E\right\}, \quad (11)$$

where N_o is Avogadro's number; λ_ψ and λ_E are coupling parameters; and the angle brackets $\langle\ \rangle$ denote an ensemble average. $\langle U^{el}(\chi_{PS})\rangle$ and $\langle N_{PS\text{-}PC}\rangle/N$ are obtained from our computer simulation. By performing the numerical integration, ΔG^{E}_{mix} can be calculated.

ΔG^{E}_{mix} is related to the excess chemical potentials of PS and PC (μ^{E}_{PS} and μ^{E}_{PC}) by

$$\Delta G^{E}_{mix} = \mu^{E}_{PS}\chi_{PS} + \mu^{E}_{PC}(1 - \chi_{PS}). \quad (12)$$

Using the Gibbs–Duhem equation, one can show that

$$\mu^{E}_{PS} = \Delta G^{E}_{mix} + (1 - \chi_{PS})d\Delta G^{E}_{mix}/d\chi_{PS},$$

and

$$\mu^{E}_{PC} = \Delta G^{E}_{mix} - \chi_{PS}d\Delta G^{E}_{mix}/d\chi_{PS}. \quad (13)$$

Thus, μ^{E}_{PS} and μ^{E}_{PC} can also be calculated numerically.

Calculation of $[Ca^{2+}]_{surf}$: mask evaluation method

The surface calcium concentration $[Ca^{2+}]_{surf}$ used in Eq. 2 can be calculated from the bulk aqueous $[Ca^{2+}]_{aq}$ using Eq. 1. Gouy–Chapman–Stern theory is used, with the assumption that the appropriate potential is that for Ca^{2+} ions that can approach to within about 2 Å of the membrane surface. For our experimental conditions, this potential is the zeta potential. Calculation of Ψ_{zeta} is straightforward (29), and the plot of Ψ_{zeta} versus χ_{PS} is shown in Fig. 1. However, if PS forms clusters in the membrane, then the local electrostatic potential surrounding PS should be higher than the average potential over the whole membrane surface. The extremes for the proper value for this local surface potential range from that for pure PS in the case of very large PS clusters, to the simple average potential for the whole bilayer surface in the case of no clusters of PS. We explored the appropriate value for the local surface potential by calculating the average *effective* mole fraction of PS around each PS molecule, $\chi_{PS,eff}$. The bilayer surface that is not close to a PS is masked off, and $\chi_{PS,eff}$ inside the mask is tabulated. This "mask evaluation" procedure works as follows:

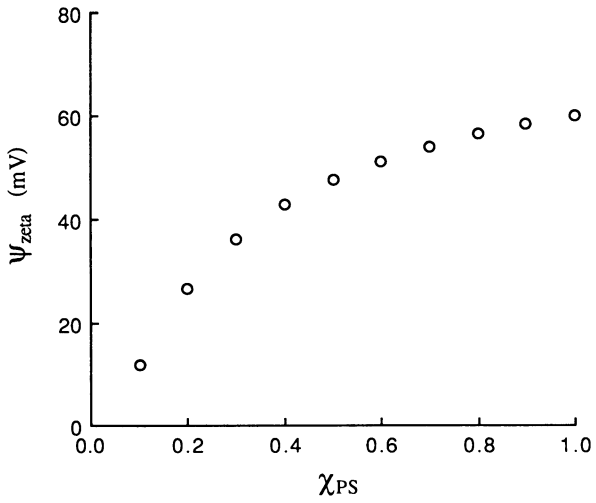

FIGURE 1 Calculated zeta potential, Ψ_{zeta}, as a function of PS mole fraction, χ_{PS}, for the experimental conditions used in this study.

(*a*) During the Monte Carlo simulation of a lipid mixture, the program counts the average number of other PS molecules within various specified distances (i.e., within the mask) from each PS. An ensemble average is calculated for each specified distance.

(*b*) For a given mask size, an effective $\chi_{PS,eff}$ is calculated using

$$\chi_{PS,eff} = \frac{\langle \text{number of PS in the mask}\rangle}{\text{number of sites in the mask}}. \quad (14)$$

(*c*) The corrected zeta potential is then calculated by the Gouy–Chapman–Stern theory using $\chi_{PS,eff}$. For ideal mixing, $\chi_{PS,eff} = \chi_{PS}$. For nonideal mixing with PS clustering, $\chi_{PS,eff} > \chi_{PS}$.

RESULTS

Measurement of Ca^{2+} binding

Fig. 2 shows the measured value of $[Ca^{2+}]_{aq}$ in equilibrium with $Ca(PS)_2$ and fluid bilayer mixtures of (16:0, 18:1)PS/PC for (14:1, 14:1)PC, (16:0, 18:1)PC, and (18:1, 18:1)PC. The value of $[Ca^{2+}]_{aq}$ required to form $Ca(PS)_2$ is seen to depend upon both χ_{PS} and also the type of PC. These measurements focussed on the lowest values of χ_{PS} that were experimentally accessible (insufficient Ca^{2+} binding was obtained at lower χ_{PS}), where electrostatic repulsion, if of sufficient magnitude relative to attractive interactions, has the most recognizable effects (see Fig. 6). For mixtures of (16:0, 18:1)PS with (14:1, 14:1)PC, measurements of equilibrium $[Ca^{2+}]_{aq}$, using essentially the same protocol as for the data in Fig.

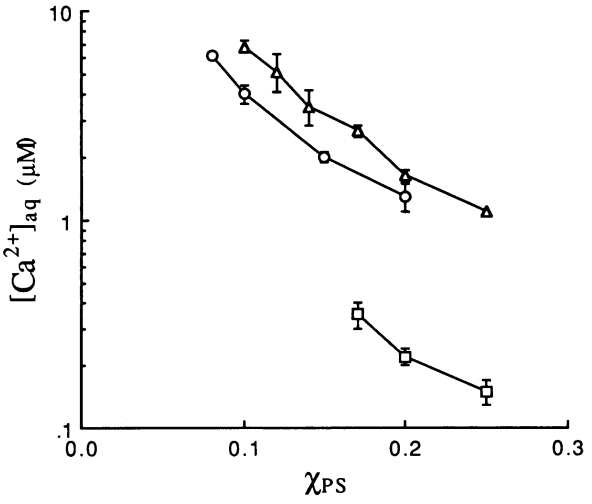

FIGURE 2 Aqueous calcium ion concentration in equilibrium with $Ca(PS)_2$ and PS/PC fluid multilamellar mixtures of PS mole fraction, χ_{PS}. (16:0, 18:1)PS is mixed with (16:0, 18:1)PC, (△); (14:1, 14:1)PC, (○); and (18:1, 18:1)PC, (□). Error bars show standard deviation that exceeds symbol size.

2, have previously been obtained from χ_{PS} = 1.0 to 0.2 (16). These earlier measurements, together with those reported in Fig. 2, were used to obtain $[Ca^{2+}]_{surf}$, as described below.

PS/PC lateral distribution

Fig. 3 shows snapshot pictures of Monte Carlo simulation of lateral distributions of PS/PC mixtures at χ_{PS} = 0.4. For clarity of presentation, the lattice size shown here is 50 × 50, although the simulations were done with 100 × 100 sites. Filled black circles represent PS, and open circles represent PC. Fig. 3 *a* shows the case of ideal mixing of PS and PC: lipids are assumed to have neither electrostatic charge nor excess nearest neighbor interaction (U^{el} and ΔE_m are both zero). The nonideality parameter ν (defined as $\nu = N_{PS-PC}(\text{observed})/N_{PS-PC}(\text{ideal})$) in this case is equal to 1.00. Fig. 3 *b* shows another hypothetical case wherein each PS has a fixed charge, but there is no other contribution to nonideal mixing ($\Delta E_m = 0$). In this case, the electrostatic repulsion between PS molecules forces them apart. There are fewer PS–PS contacts and more PS–PC contacts than in the ideal mixing case, as quantified by the higher nonideality parameter, ν = 1.07. If ΔE_m is chosen as +0.2 kT, with each PS having a fixed charge, the distribution looks ideal (simulation not shown) with ν = 1.00. Fig. 3 *c–e* show PS/PC mixtures at ΔE_m = +0.6, +0.8, and +1.0 kT, respectively, all including fixed charge on PS. Clusters of like lipids are increasingly apparent as ΔE_m increases. The nonideality parameter in these cases is 0.78, 0.63, and 0.46, respectively.

The size of clusters of like lipid is dependent not only on the nonideal energy ΔE_m, but also on the mole fraction of PS. This is illustrated in Fig. 4, where ΔE_m is held constant at 0.8 kT as χ_{PS} varies from 0.1 to 0.9.

Excess free energy calculation

To make a direct comparison of computer simulation results with calcium binding experiments, we calculated the excess Gibbs free energy for nonideal mixing (see Appendix for details). Fig. 5 shows the excess Gibbs free energy of PS/PC mixtures versus χ_{PS}. When lipids mix ideally, excess Gibbs free energy is zero at all χ_{PS} values. For PS/PC bilayers, ΔG^E_{mix} is negative from ΔE_m = 0 to about 0.2 kT, and positive for $\Delta E_m \geq 0.3$ kT.

Fig. 6 shows ln γ versus χ_{PS} (i.e., μ^E/RT versus χ_{PS}) for PS and PC, calculated using Eq. 13. A comparison of ln γ_{PS} versus χ_{PS} from the experimental measurements and from the computer simulations is made in Fig. 7. Using Eqs. 1 and 2, ln $\gamma_{PS,exp}$ was calculated from the equilibrium $[Ca^{2+}]_{aq}$ from Fig. 2 and the data from Fig. 2 of Swanson and Feigenson (16) for (16:0, 18:1)PS/(14:1, 14:1)PC. The Gouy–Chapman–Stern calculation of $[Ca^{2+}]_{surf}$ was used to find the values of ln $\gamma_{PS,exp}$ that are plotted as the upper data points (○), and the computer-simulated ln $\gamma_{PS,calc}$ for ΔE_m = +0.4 and +0.6 kT are drawn as continuous lines. As χ_{PS} decreases, ln $\gamma_{PS,exp}$ increases monotonically, starting from ln $\gamma_{PS,exp}$ = 0 at χ_{PS} = 1 to ln $\gamma_{PS,exp}$ = 1.3 at χ_{PS} = 0.15.

Mask evaluation of local surface potential

The Gouy–Chapman–Stern double layer theory used to calculate $[Ca^{2+}]_{surf}$ is a smeared charge model theory. When PS forms clusters, the local electrostatic potential near the PS clusters should be higher than the potential averaged over the membrane surface, hence the local $[Ca^{2+}]_{surf}$ near a PS cluster will also be higher than the average $[Ca^{2+}]_{surf}$ over the whole membrane. Then, from Eq. 1 and 2, the actual ln γ_{PS} should be lower than that calculated by using Gouy–Chapman–Stern theory to find $[Ca^{2+}]_{surf}$. We used the "mask evaluation" method described in the Materials and Methods section to explore the effect of the clustering of PS. Fig. 8 shows the computer-simulated effective PS mole fraction $\chi_{PS,eff}$ versus χ_{PS}, at mask size 6 and 18. Note that $\chi_{PS,eff}$ depends strongly on the non-electrostatic excess mixing energy ΔE_m. For a nearly ideal mixing case, such as ΔE_m = 0.2 kT, $\chi_{PS,eff}$ is almost the same as χ_{PS}. As ΔE_m increases, $\chi_{PS,eff}$ becomes significantly larger than χ_{PS}. For example, with mask size 6, for ΔE_m = 0.8 and χ_{PS} = 0.3, the calculated $\chi_{PS,eff}$ is about 0.5. The mask size also plays an important role. The largest $\chi_{PS,eff}$ occurs at the smallest mask size. As mask size increases, the difference between $\chi_{PS,eff}$ and χ_{PS} decreases. In the limit of an infinitely large mask, $\chi_{PS,eff}$ becomes equal to χ_{PS}: we go back to the smeared charge model.

Our objective is to find a ΔE_m such that the $\chi_{PS,eff}$ will give a ln $\gamma_{PS,exp}$ (from Eqs. 1 and 2), which is the same as

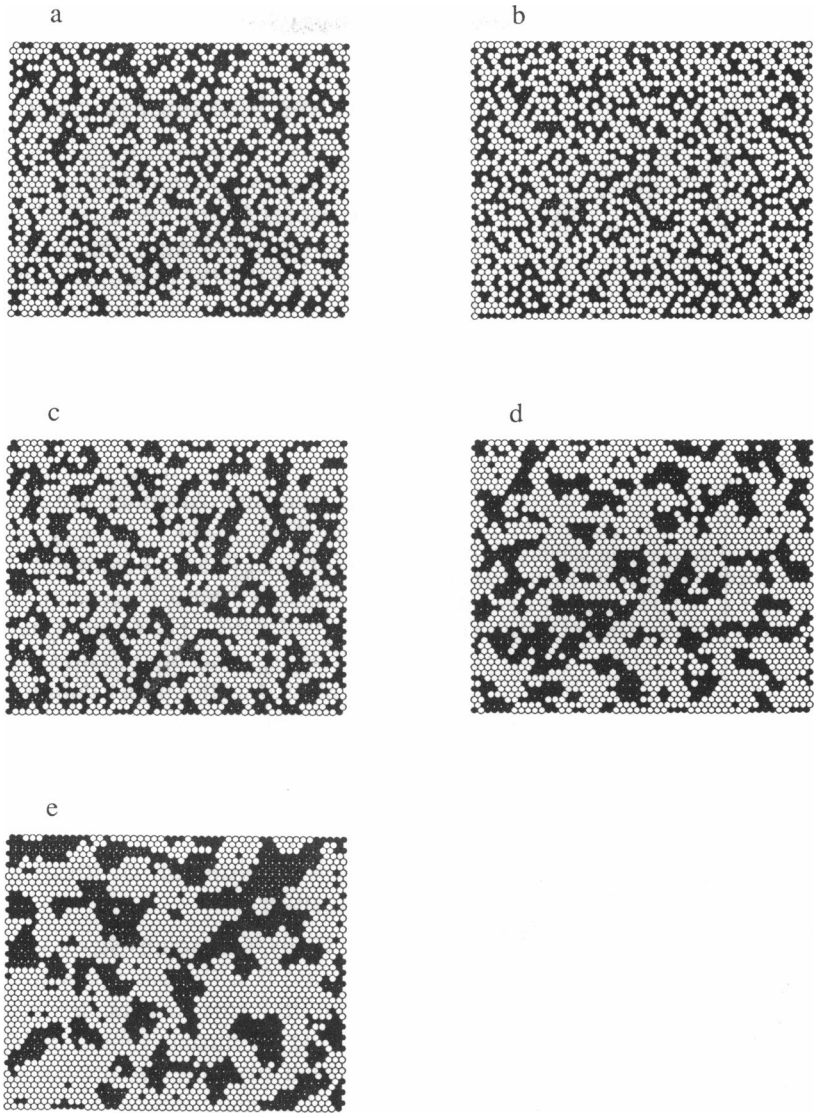

FIGURE 3 Snapshot pictures of the lateral distribution of PS/PC mixtures at $\chi_{PS} = 0.4$ for various assumed PS–PC interactions. (*a*) ideal mixing: no excess interaction energy; (*b–e*) repulsive interaction with each PS having fixed negative charge. (*b*) non-electrostatic excess mixing energy, $\Delta E_m = 0$ kT; (*c*) $\Delta E_m = 0.6$ kT; (*d*) $\Delta E_m = 0.8$ kT; (*e*) $\Delta E_m = 1.0$ kT. PS, (●); PC, (○).

the ln $\gamma_{PS,calc}$ associated with this ΔE_m from the computer simulation. The procedure we use is as follows:

(*a*) Choose a mask size.
(*b*) Pick an initial reasonable ΔE_m value (e.g., 0.5 kT).
(*c*) Find the $\chi_{PS,eff}$ associated with this ΔE_m from the computer simulation data.
(*d*) Find the zeta potential associated with this $\chi_{PS,eff}$ and use this potential to find $[Ca^{2+}]_{surf}$, and ln $\gamma_{PS,exp}$.
(*e*) Find a new ΔE_m value from computer simulation data that will yield ln $\gamma_{PS,calc}$ = ln $\gamma_{PS,exp}$.
(*f*) If the new value of ΔE_m differs from the old one, use the new value for ΔE_m, and repeat steps (*c*)–(*e*).

This procedure is found to converge quickly. The reason for rapid convergence is that if the initial ΔE_m is larger than that which actually corresponds to the experimental result, then this large ΔE_m results in a high $\chi_{PS,eff}$, hence a high $[Ca^{2+}]_{surf}$ and a low ln $\gamma_{PS,exp}$, and eventually a lower new ΔE_m. This negative feedback property insures a rapidly converging solution. Values of ln $\gamma_{PS,exp}$ for the (16:0, 18:1-PS)/(14:1, 14:1-PC) lipid mixture calculated with a mask size of 6 are also plotted in Fig. 7. The values obtained using the small mask size are consistently lower than those calculated simply with Gouy–Chapman–Stern theory. The ln $\gamma_{PS,exp}$ values calculated with larger mask sizes fall between those for mask size 6 and Gouy–Chapman–Stern treatment.

Fig. 9 shows a comparison of ln γ_{PS} of (16:0, 18:1)PS in binary mixtures with (16:0, 18:1)PC, (14:1, 14:1-PC), or (18:1, 18:1)PC. The mask size used is 18. The mixture with (16:0, 18:1)PC shows the lowest ln $\gamma_{PS,exp}$,

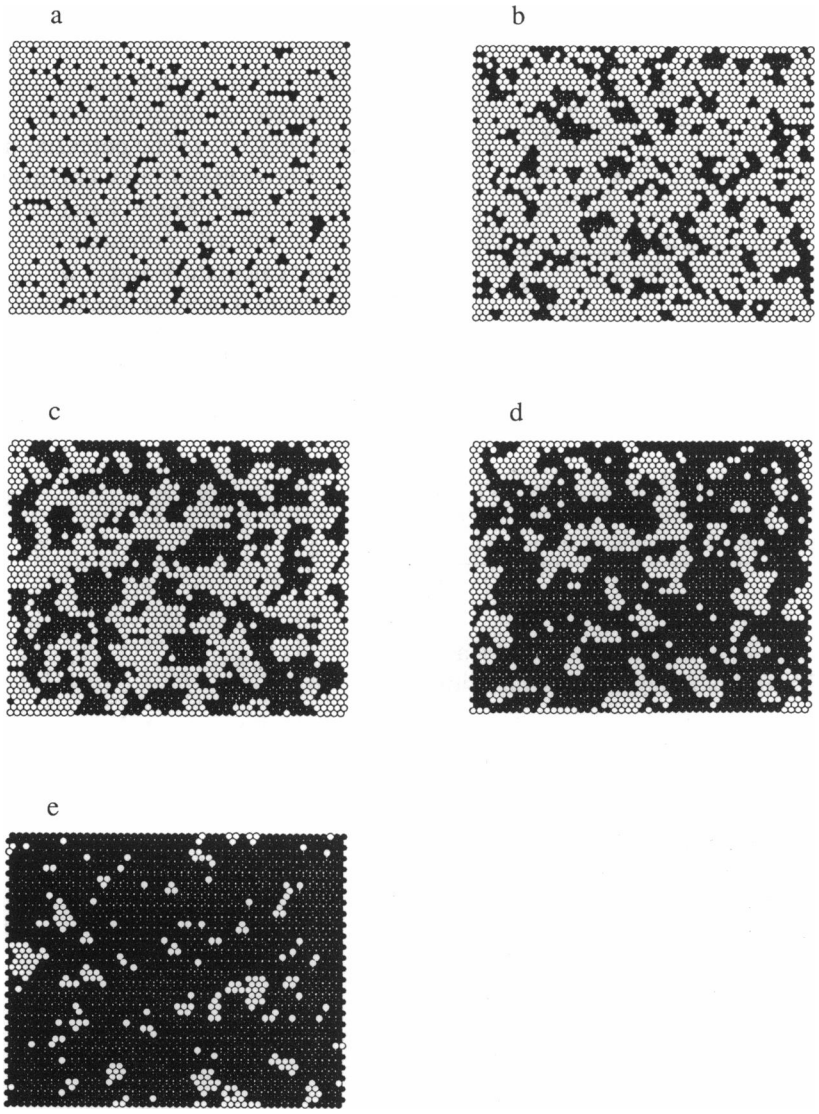

FIGURE 4 Snapshot pictures of the lateral distribution of PS/PC mixtures with ΔE_m = 0.8 kT show nonideal mixing as a function of PS mole fraction. (*a*) χ_{PS} = 0.1; (*b*) χ_{PS} = 0.3; (*c*) χ_{PS} = 0.5; (*d*) χ_{PS} = 0.7; (*e*) χ_{PS} = 0.9. PS, (●); PC, (○).

with a slightly higher ln $\gamma_{PS,exp}$ for the mixture with (14:1, 14:1)PC. The ΔE_m value corresponding to these mixtures is 0.4–0.5 kT. However, ln $\gamma_{PS,exp}$ of mixtures with (18:1, 18:1)PC are higher than for the other two mixtures, with ΔE_m approximately 0.8 kT.

DISCUSSION

Experimental

This study relies on the measurement of a Ca^{2+} concentration that is in equilibrium in the heterogeneous chemical reaction $Ca^{2+} + 2PS^- \rightleftharpoons Ca(PS)_2$. These thermodynamic studies do not provide information about the detailed mechanism of the reaction. For example, the reaction might proceed in two steps, such as, (*a*) $Ca^{2+} + PS^- \rightleftharpoons Ca^{2+} - PS^-$ followed by (*b*) $Ca^{2+} - PS^- + PS^- \rightleftharpoons Ca(PS)_2$. Regardless of the mechanism, these studies provide information about the chemical potential of the reactant, PS, in a fluid lamellar phase.

However, if a significant fraction of the PS in the *fluid* lamellar phase were to bind Ca^{2+}, or else if the ionic strength were to vary among the samples, then our treatment would require modification. Ca^{2+} binding to the fluid phase PS can be determined (29), and the ionic strength is easily calculated. At χ_{PS} = 1.0, at the equilibrium $[Ca^{2+}]_{aq}$ of 41 nM, the fraction of PS in the fluid phase *without* bound Ca^{2+} is 0.9999. The ionic strength is 113.0 mM. At χ_{PS} = 0.10, at an equilibrium $[Ca^{2+}]_{aq}$ of 6 μM, the fraction of PS in the fluid phase *without* bond Ca^{2+} is 0.9996. The ionic strength is 112.7 mM. Since these represent the extremes of the differences in

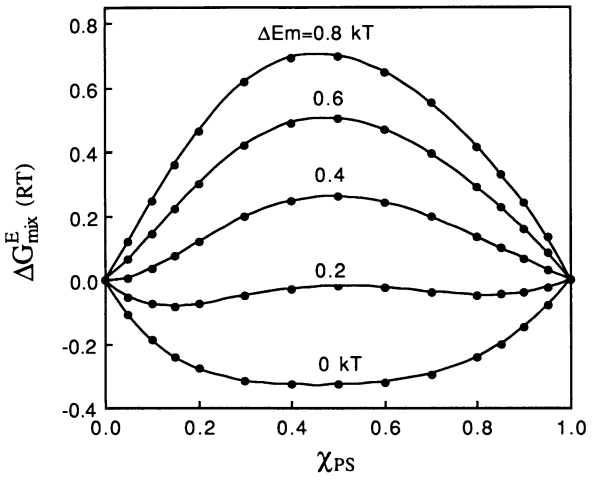

FIGURE 5 Excess Gibbs free energy of mixing, ΔG^E_{mix}, units of RT, as a function of χ_{PS} for a repulsive electrostatic interaction for PS, and various values of the non-electrostatic excess mixing energy, ΔE_m.

all of our samples, we conclude that the effects of Ca^{2+} binding to fluid phase PS and of ionic strength variation are small.

The principal experimental result is that the activity coefficient of PS (and of PC) in the fluid PS/PC bilayer is greater than unity (with a standard state for pure PS defined with $\gamma_{PS} \equiv 1.0$). This type of nonideal mixing means that contacts between like lipids are of lower energy than are contacts between unlike lipids: like lipids are clustered. This result is surprising, since the most apparent interaction is the electrostatic repulsion between the negatively charged PS. That this repulsion is overcome means that there are less-apparent interactions that favor contact of like lipids. Our experiments do not reveal the nature of these interactions. Possibilities include: (*a*) packing of PC and/or packing of PS that gives favorable dipole–dipole, ion–dipole, or dispersion interactions, but which is a sufficiently different type of packing for the two types of lipids; (*b*) packing of PS and/or packing of PC that gives favorable interactions with water, but is sufficiently different for the two types of headgroups; and (*c*) a 2-dimensional hydrogen bonding network among the PS headgroups.

Computer simulations

The implications of the experimental results were explored by means of computer simulation of the lateral lipid distribution.

Calculation of $[Ca^{2+}]_{surf}$ from the measured $[Ca^{2+}]_{aq}$

The reaction we utilize is between membrane-bound PS and Ca^{2+}. Because of the negative electrostatic potential of the PS^--containing membranes, $[Ca^{2+}]_{surf}$ is greater than $[Ca^{2+}]_{aq}$, the concentration of Ca^{2+} that we measure in the bulk aqueous medium. The well-known form of this correction, Eq. 1, takes account of the electrostatically-driven accumulation of Ca^{2+}. For a uniform, smeared charge distribution, a reasonable value for Ψ is the average value for the whole membrane at closest approach of Ca^{2+} to the potential-determining layer, i.e., a few Å above the surface. This average value can be calculated from the surface charge density or from a measured value of the zeta potential. We have used these procedures to calculate Ψ and $[Ca^{2+}]_{surf}$. However, if the negative charge is located in patches, then the surface potential that is effective in causing Ca^{2+} accumulation might be larger than the average surface potential. We have no *a priori* theory for the number of neighbors around a

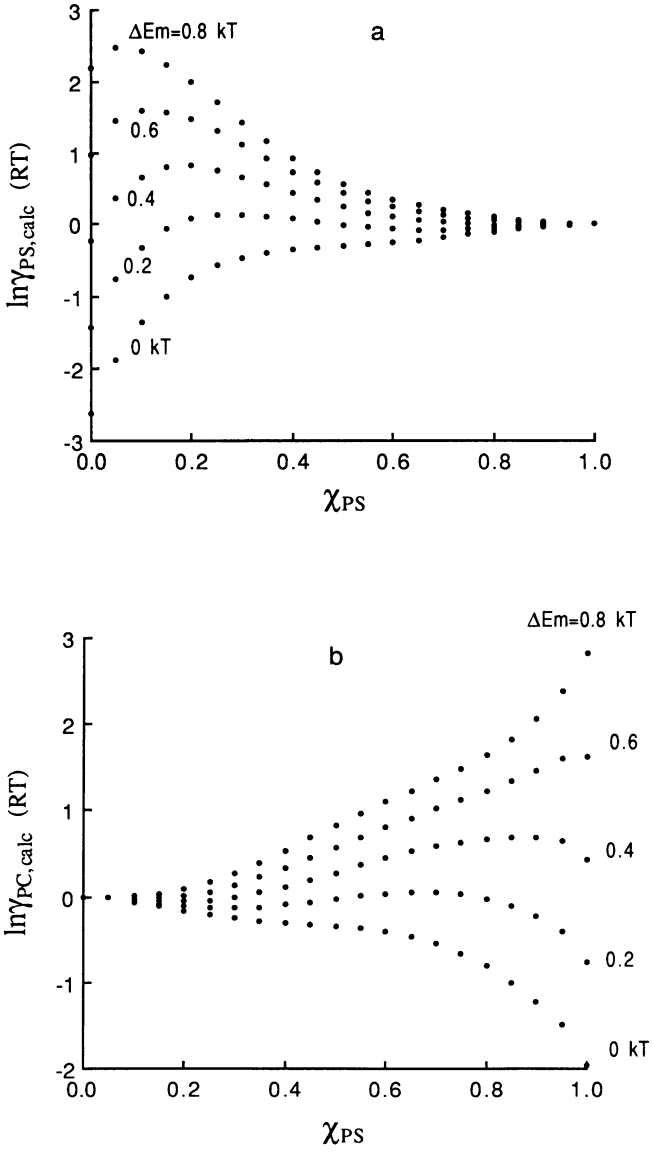

FIGURE 6 Calculated excess chemical potential as a function of χ_{PS} at various values of the non-electrostatic excess mixing energy, ΔE_m. (*a*) $\ln \gamma_{PS,calc}$; (*b*) $\ln \gamma_{PC,calc}$.

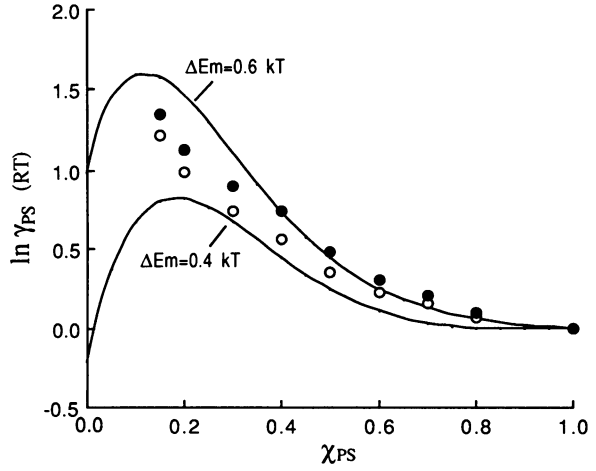

FIGURE 7 Comparison of the experimental and the computer-simulated values of excess chemical potential of PS, ln γ_{PS}. Computer-simulated ln $\gamma_{PS,calc}$ for ΔE_m = 0.4 and 0.6 kT are drawn as continuous lines. ln $\gamma_{PS,exp}$ for (16:0, 18:1-PS)/(14:1, 14:1-PC) lipid mixtures are plotted as symbols: calculated with Gouy–Chapman–Stern theory, (○); calculated with mask evaluation method, using mask size 6, (●). Mean values of the raw data shown in Fig. 1, and Fig. 2 of Swanson and Feigenson (16), are used for these calculations.

given PS molecule that would contribute to the potential experienced by Ca^{2+} ions near the PS. However, because we obtain a simulated representation of the PS/PC distribution, we could explore this question, using the "mask evaluation" method described in Materials and Methods. Fig. 7 shows that the most simple assumption of smeared charge gives a value for ln $\gamma_{PS,exp}$ that is only slightly greater than that calculated for the largest reasonable value of the membrane potential near a PS, obtained using the "nearest-neighbor-sized" mask size of 6. Thus, the "mask evaluation" method implies that the calculation of $[Ca^{2+}]_{surf}$ does not suffer from a serious error caused by local variation of Ψ.

Model for U^{el}

Our model for the basis of nonideal mixing divides the excess energy of mixing into an electrostatic term, U^{el}, and a term ΔE_m that includes all other, shorter range, interactions. Making this division of the excess interaction energy allows us to calculate the long-range electrostatic repulsion contribution, and then to allow only the ΔE_m term to vary, until a match is found between ln $\gamma_{PS,exp}$ and ln $\gamma_{PS,calc}$. We recognize that the value of U^{el} that we calculate is dependent upon the details of our model. For example, an increase in any of the dielectric constants, or a location of the negative PS charges closer to the high dielectric constant region, would decrease the value of U^{el}. Nonetheless, the final result remains, that the electrostatic repulsion is exceeded by attractive interaction. If we err by underestimating U^{el}, then both the actual repulsion and the actual attraction must be larger. From Fig. 7 we see that U^{el} is evident as a downward curvature, a decrease in ln $\gamma_{PS,calc}$ at low χ_{PS}. Therefore, Ca^{2+} binding data as χ_{PS} approaches zero are most useful for testing our model for U^{el}. However, our data extend only as low as χ_{PS} = 0.15 for (18:1, 18:1)PC, and to χ_{PS} = 0.1 for (14:1, 14:1)PC and (16:0, 18:1)PC. Even though we emphasized obtaining data in the low χ_{PS} regime, Ca^{2+} binding is much weaker, varying approximately as $(\chi_{PS})^{-2}$, so reliable data are difficult to obtain. Nonetheless, we can say that U^{el} is probably not much greater than we have calculated, since we would then expect to have detected the predicted downward curvature of ln $\gamma_{PS,cal}$ versus χ_{PS} at low χ_{PS}. But, U^{el} might be

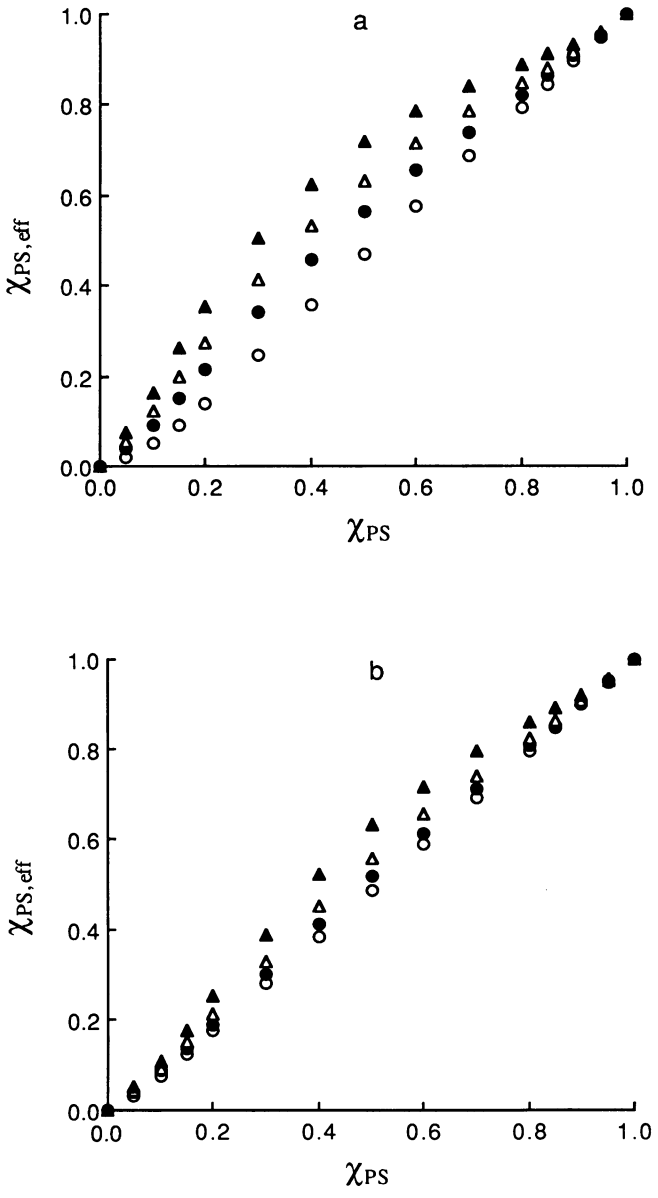

FIGURE 8 Effective PS mole fraction, $\chi_{PS,eff}$, as a function of χ_{PS} at various mask sizes and values of the non-electrostatic excess mixing energy, ΔE_m. ΔE_m = 0 kT, (○); 0.4 kT, (●); 0.6 kT, (△); and 0.8 kT, (▲). (*a*) mask size 6; (*b*) mask size 18.

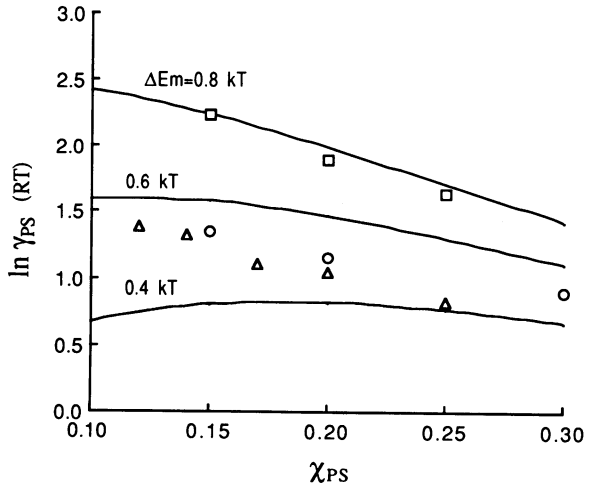

FIGURE 9 Comparison of the experimental and the computer-simulated values of excess chemical potential of PS, ln γ_{PS}. Computer-simulated ln $\gamma_{PS,calc}$ for ΔE_m = 0.4, 0.6 and 0.8 kT are drawn as continuous lines. Experimental values ln $\gamma_{PS,exp}$ are for (16:0, 18:1)PS in lipid mixtures with (16:0, 18:1)PC, (△); (14:1, 14:1)PC, (○); and (18:1, 18:1)PC, (□). All ln $\gamma_{PS,exp}$ are calculated with the mask evaluation method using mask size 18.

smaller than we have calculated, since our experiments would not have detected this. This could occur, for example, if the PS–PS repulsion were attenuated by a larger dielectric constant than we assumed, or by the location of the negative charges closer to the aqueous region. Also, if the polar region, where we set ϵ = 30, actually has a gradient, e.g., from ϵ = 2 to 78, and if the charged moieties are not too strongly restricted in location, then the charges would tend to move toward a location with higher dielectric constant. Finally, the PS headgroup actually has one full positive charge and one full negative charge, in addition to the net partial negative charge that we have treated here. We plan to study details of this model of electrostatic interactions in future experiments directed toward still lower values of χ_{PS}.

We have placed all interactions, attractive or repulsive, that would be different between like and unlike lipids pairs, in the ΔE_m term (with the exception of point charge repulsion). This is reasonable for the purpose of calculation, since such interactions are all shorter range than is point charge repulsion, and so can be tabulated together in the computer simulation by counting the number of PS–PC pairs. We note that this assumption, that the excess interaction energy is pairwise additive, remains to be tested. Additivity might not be a good description, for example, of hydrogen bonds or of reorienting neighboring dipoles.

In Fig. 5, we see that when ΔE_m is greater than about 0.3 kT, it dominates over U^{el} in contributing to ΔG^E_{mix}: lipid mixtures show positive deviation from ideality. However, because of the long-range nature of the electrostatic interaction, the repulsive contribution can be seen even at high ΔE_m. For example, when PS comprises 10% of the PS/PC mixture, the PS clusters are barely noticeable (Fig. 4 *a*); in contrast, when PC comprises 10% of the PS/PC mixture, the PC clusters are clearly apparent (Fig. 4 *e*). The nonideality parameter ν is 0.93 for the dilute PS in Fig. 4 *a*, and 0.66 for the more clustered PC in Fig. 4 *e*. A similar situation is found for mixtures with, for example, χ_{PS} = 0.3 and 0.7 (Fig. 4 *b* and 4 *d*). If the nearest neighbor nonideal interaction ΔE_m were the only excess interaction in the mixture, we would expect a symmetry of ν about the midpoint of composition. The breaking of symmetry is the direct result of the long-range nature of the electrostatic interaction: at high PS mole fraction, the charge particle density is high, and spatial variation of electrostatic potential is small. PC molecules can form clusters to reduce PS–PC contacts without significantly affecting the total electrostatic energy. In contrast, at low PS mole fraction, the charge particle density is low, and the discreteness of charge shows up. PS molecules keep a distance from each other. This effect is also shown in Fig. 6, where ln $\gamma_{PS,calc}$ decreases as χ_{PS} approaches zero. Another effect of electrostatic interaction is that the shapes of PS clusters are irregular and thinner, compared to a case with no electrostatic interaction. PS molecules avoid forming thick, round clusters due to electrostatic repulsion.

How nonideal is mixing of PS/PC?

We find ΔE_m for (14:1, 14:1)PC and for (16:0, 18:1)PC to be 0.4–0.5 kT, and for (18:1, 18:1)PC about 0.8 kT, all in mixtures with (16:0, 18:1)PS. ΔE_m is a composite of attractive and repulsive interactions: its magnitude is not readily interpretable in molecular terms. However, the calculation of ΔG^E_{mix} is revealing. For simplicity, since the free energy is composition-dependent, we focus comparison at χ_{PS} = 0.5. Here, for mixtures with (14:1, 14:1)PC and (16:0, 18:1)PC, ΔG^E_{mix} = 0.25–0.4 RT. For mixtures with (18:1, 18:1)PC, $\Delta G^E_{mix} \approx$ 0.7 RT. This latter value would *require* a phase separation at an overall χ_{PS} = 0.5, with two phases having different χ_{PS}! This phase separation requirement is a consequence of the *maximum possible* value of ΔG^E_{mix} = (ln 2) RT for a binary mixture at χ = 0.5. In fact, regular solution theory as well as other mixing models (18) yield a maximum for ΔG^E_{mix} of $\sim$ 0.5 RT at χ = 0.5. We did not find a phase separation in the limited experimental range of χ_{PS} = 0.15–0.25 for (16:0, 18:1)PS/(18:1, 18:1)PC. Experiments are underway to test the entire range of χ_{PS}. Phase separation would be revealed by a constant value of $[Ca^{2+}]_{aq}$ versus χ_{PS} (i.e., loss of one degree of freedom) in the region where two fluid bilayer phases coexist.

Whereas in principle our canonical ensemble with Kawasaki relaxation should reveal any cases of the equilibrium of two coexisting phases, together with the corresponding correct value of ΔG^E_{mix}, in fact the number of simulations required increases enormously when there is

phase separation. For example, Rovere et al. (42) found 800,000 steps to be *insufficient* to properly represent phase separation in a 2-dimensional system, using a canonical ensemble. They suggest using either a grand canonical ensemble or a Gibbs ensemble, methods which might also be appropriate for our system to properly characterize phase separation. Since the method we use overestimates the energy when two phases are present (by including the interfacial contribution), the value of ΔG^{E}_{mix} in a two-phase region, as well as the position of the phase boundaries, would not be determined properly. However, we point out that we are not in danger of missing the fact of phase separation, but rather its accurate description: the shape of the plot of ΔG^{total} versus χ_{PS} (i.e., if $\partial^2 \Delta G^{total}/\partial \chi^2_{PS} \leq 0$) would reveal any phase separation (18), and our simulation does come to equilibrium in the one-phase regions.

SUMMARY

1. High-affinity Ca^{2+} binding measurements can be used to determine the activity coefficients of PS and PC in fluid bilayer mixtures.
2. The free energy can be calculated for a simulated lateral distribution of PS and PC by use of Kirkwood's coupling parameter method. A simulated distribution can then be found, with a calculated free energy that corresponds to the experimental results.
3. Mixing of PS and PC is nonideal, with PS and PC clustered rather than randomly distributed, despite the electrostatic repulsion between PS headgroups.
4. Mixing of PS and PC can be modeled to take account explicitly of the electrostatic energy.
5. The long-range electrostatic repulsion gives a different character to PS clusters compared to PC clusters: PS clusters are less compact and form less readily than PC clusters.
6. A "masked evaluation" method was developed in order to explore the non-uniform surface charge that follows PS clustering. A modest increase in the surface Ca^{2+} concentration is found near the PS clusters, compared to the Ca^{2+} concentration averaged over the entire bilayer surface.

APPENDIX

Derivation of the excess Gibbs free energy of a PS/PC mixture using the Kirkwood coupling parameter method

From Eq. 10 we have

$$\Delta G^{E}_{mix} = g^{res}_{mix} - g^{res}_{pure\ PC} - \chi_{PS}(g^{res}_{pure\ PS} - g^{res}_{pure\ PC}). \quad (A1)$$

Based on our model of the PS/PC lipid mixture, the term $(g^{res}_{pure\ PS} - g^{res}_{pure\ PC})$ has a simple meaning: for each pure lipid, configuration entropy (which is the only entropy contribution included in our model) is the same. The free energy difference is therefore just the difference of energies of these two pure states. Thus, from the expression for the total energy, Eq. 5, we have

$$\chi_{PS}(g^{res}_{pure\ PS} - g^{res}_{pure\ PC}) = \chi_{PS}[(U_{PS\text{-}PS} - U_{PC\text{-}PC})ZN_o/2 + N_o U^{el}(\chi_{PS} = 1)/N], \quad (A2)$$

where N_o is Avogadro's number.

In order to calculate $g^{res}_{mix} - g^{res}_{pure\ PC}$, we now introduce three coupling parameters: λ_A, λ_ψ, and λ_E. Eq. 5 can then be modified to describe the energy for one mole of mixture with three coupling parameters:

$$U^{T}(\lambda_A, \lambda_\psi, \lambda_E) = ZN_o\chi_{PS}U_{PC\text{-}PC}\lambda_A/2 + ZN_o\chi_{PC}U_{PC\text{-}PC}/2 + N_o(N_{PS\text{-}PC}/N)\lambda_E + \lambda_\psi N_o U^{el}(\chi_{PS})/N. \quad (A3)$$

By continuously varying the coupling parameters, we can convert the system from pure PC to a PS/PC mixture. The difference in free energy

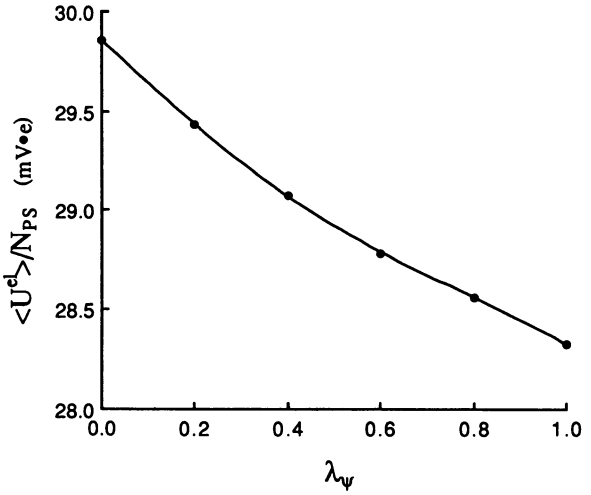

FIGURE A1 Electrostatic component of the calculation of ΔG^{E}_{mix}: Canonical ensemble average of $\langle U^{el}\rangle/N_{PS}$ versus coupling parameter λ_ψ at $\chi_{PS} = 0.4$.

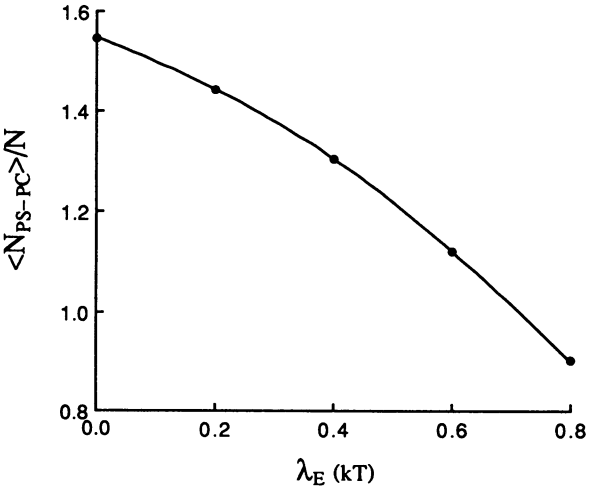

FIGURE A2 Non-electrostatic component of the calculation of ΔG^{E}_{mix}: Canonical ensemble average of $\langle U_{PS\text{-}PC}\rangle/N$ versus coupling parameter λ_E at $\chi_{PS} = 0.4$.

of two states is independent of the integral path used, so we can choose the following convenient integral path (i.e., charging process) as follows: (*a*) begin with a pure PC system, i.e., $(\lambda_A, \lambda_\psi, \lambda_E) = (1, 0, 0)$; (*b*) gradually change λ_A from 1 to the ratio $U_{PS\text{-}PS}/U_{PC\text{-}PC}$, i.e., $(\lambda_A, \lambda_\psi, \lambda_E) = (U_{PS\text{-}PS}/U_{PC\text{-}PC}, 0, 0)$. In this state, PS and PC are distinguished by their own interaction energies, $U_{PS\text{-}PS}$ and $U_{PC\text{-}PC}$, but there are no nonideal nearest neighbor interactions and no long-range electrostatic interactions in the mixture; (*c*) gradually increase the electrostatic interaction by varying λ_ψ from 0 to 1, i.e., $(\lambda_A, \lambda_\psi, \lambda_E) = (U_{PS\text{-}PS}/U_{PC\text{-}PC}, 1, 0)$. The PS in the lipid mixture has an electrostatic charge, but there is no other nonideal nearest neighbor interaction; (*d*) finally, allow the system to have the nonideal interaction energy ΔE_m, i.e., $(\lambda_A, \lambda_\psi, \lambda_E) = (U_{PS\text{-}PS}/U_{PC\text{-}PC}, 1, \Delta E_m)$. At this point, the PS/PC mixture has all the interactions expressed in Eq. 5. Applying the Kirkwood coupling parameter method (38), the free energy difference can be calculated by using the above three charging processes:

$$g^{res}_{mix} - g^{res}_{pure\ PC} = \int_1^{U_{PS\text{-}PS}/U_{PC\text{-}PC}} \langle \partial U^T/\partial\lambda_A \rangle \, d\lambda_A \Big|_{\lambda_\psi=0,\ \lambda_E=0}$$
$$+ \int_0^1 \langle \partial U^T/\partial\lambda_\psi \rangle \, d\lambda_\psi \Big|_{\lambda_A=U_{PS\text{-}PC}/U_{PC\text{-}PC},\ \lambda_E=0}$$
$$+ \int_0^{\Delta E_m} \langle \partial U^T/\partial\lambda_E \rangle \, d\lambda_E \Big|_{\lambda_A=U_{PS\text{-}PS}/U_{PC\text{-}PC},\ \lambda_\psi=1}$$
$$= (U_{PS\text{-}PS} - U_{PC\text{-}PC}) Z N_o \chi_{PS}/2 + N_o/N \int_0^1 \langle U^{el}(\chi_{PS}) \rangle \, d\lambda_\psi \Big|_{\lambda_E=0}$$
$$+ N_o \int_0^{\Delta E_m} \langle N_{PS\text{-}PC} \rangle \Big|_{\lambda_\psi=1} \Big/ N \, d\lambda_E. \quad (A4)$$

Combining Eqs. A1, A2, and A4, the molar excess Gibbs free energy of a PS/PC mixture is finally given by:

$$\Delta G^E_{mix} = N_o \left\{ \left[\int_0^1 \langle U^{el}(\chi_{PS}) \rangle \, d\lambda_\psi \Big|_{\lambda_E=0} - \chi_{PS} U^{el}(\chi_{PS} = 1) \right] \Big/ N + \int_0^{\Delta E_m} \langle N_{PS\text{-}PC} \rangle \Big|_{\lambda_\psi=1} \Big/ N \, d\lambda_E \right\}, \quad (A5)$$

where the ensemble averages $\langle U^{el}(\chi_{PS}) \rangle$ and $\langle N_{PS\text{-}PC} \rangle / N$ can be directly obtained from computer simulation. Note that although λ_A was involved in the derivation, it does not appear in the final form, Eq. A5. Thus, ΔG^E_{mix} can be determined through two independent charging processes corresponding to the coupling parameters λ_ψ and λ_E.

The components of this calculation are shown separately in Figs. A1 and A2, wherein we give an example, at $\chi_{PS} = 0.4$, of the canonical ensemble average of $\langle U^{el}(\chi_{PS}) \rangle / N_{PS}$ and $\langle N_{PS\text{-}PC} \rangle / N$ versus coupling parameters λ_ψ and λ_E. $U^{el}(\chi_{PS})$ was calculated according to Eq. 8. The electrostatic contribution of charges within five lipid diameters from a PS was directly obtained from simulation using the discrete charge treatment. More distant electrostatic effects were treated as smeared charge using the cutoff disk method of Levine (43, 44). Because of the large cutoff disk size (about 85 Å in diameter), charges outside the disk contribute only a few percent to U^{el}. Each point in Figs. A1 and A2 was the average of three independent Monte Carlo simulations with corresponding coupling parameters. The data points were first fit to a polynomial, and then numerically integrated according to Eq. A5.

We wish to thank S. McLaughlin for helpful comments and for measurements of electrophoretic mobility.

This work was supported by National Institutes of Health grant HL-18255 and National Science Foundation grant DMB-89-12912. A. R. G. Dibble and A. K. Hinderliter were supported in part by National Institutes of Health Research Service Award 5T32GM-07273.

Received for publication 24 August 1992 and in final form 26 October 1992.

REFERENCES

1. Sweet, W. D., and F. Schroeder. 1988. Lipid domains and enzyme activity. *In* Lipid Domains and the Relationship to Membrane Function. R. C. Aloia, C. C. Curtain, and L. M. Gordon editors. Alan R. Liss, Inc., New York. 17–42.
2. Thompson, T. E., M. B. Sankaram, and R. L. Biltonen. 1992. Biological membrane domains: functional significance. *Comm. Mol. Cell. Biophys.* 8:1–15.
3. Wolf, D. E. 1992. Lipid domains: the parable of the blind man and the elephant. *Comm. Mol. Cell. Biophys.* 8:83–95.
4. Edidin, M. 1990. Molecular associations and membrane domains. *Curr. Top. Membr. Trans.* 36:81–96.
5. Kinnunen, P. K. J. 1991. On the principles of functional ordering in biological membranes. *Chem. Phys. Lipids.* 57:375–399.
6. Mabrey, S., and J. M. Sturtevant. 1976. Investigation of phase transitions of lipids and lipid mixtures by high sensitivity differential scanning calorimetry. *Proc. Natl. Acad. Sci. USA.* 73:3862–3866.
7. Tenchov, B. G. 1985. Nonuniform lipid distributions in membranes. *Prog. Surf. Membr. Sci.* 20:273–340.
8. Lee, A. G. 1977. Lipid phase transitions and phase diagrams. II. Mixtures involving lipids. *Biochim. Biophys. Acta.* 472:285–344.
9. Ipsen, J. H., and O. G. Mouritsen. 1988. Modeling the phase equilibria in two-component membranes of phospholipids with different acyl-chain lengths. *Biochim. Biophys. Acta.* 944:121–134.
10. Cheng, W. H. 1980. A theoretical description of phase diagrams for nonideal lipid mixtures. *Biochim. Biophys. Acta.* 600:358–366.
11. Shin, Y.-K., and J. H. Freed. 1989. Dynamic imaging of lateral diffusion by electron spin resonance and study of rotational dynamics in model membranes. Effect of cholesterol. *Biophys. J.* 55:537–550.
12. Hartley, G. S., and J. W. Roe. 1940. Ionic concentrations at interfaces. *Trans. Farad. Soc.* 36:101–109.
13. Cafiso, D., A. McLaughlin, S. McLaughlin, and A. Winiski. 1989. Measuring electrostatic potentials adjacent to membranes. *Methods Enzymol.* 171:342–364.
14. Fromherz, P. 1989. Lipid coumarin dye as a probe of interfacial electrical potential in membranes. *Methods Enzymol.* 171:371–387.
15. Feigenson, G. W. 1989. Calcium ion binding between lipid bilayers: The four-component system of phosphatidylserine, phos-

phatidylcholine, calcium chloride, and water. *Biochemistry.* 28:1270–1278.

16. Swanson, J. E., and G. W. Feigenson. 1990. Thermodynamics of mixing of phosphatidylserine/phosphatidylcholine from measurements of high-affinity calcium binding. *Biochemistry.* 29:8291–8297.
17. Nagle, J. F., and M. C. Weiner. 1988. Structure of fully hydrated bilayer dispersions. *Biochim. Biophys. Acta.* 942:1–10.
18. Guggenheim, E. A. 1952. Mixtures. Clarendon Press, Oxford.
19. Brown, R. H. 1974. Membrane surface charge: discrete and uniform modelling. *Prog. Biophys. Mol. Biol.* 28:343–370.
20. Nelson, A. P., and D. A. McQuarrie. 1975. The effect of discrete charges on the electrical properties of a membrane. 1. *J. Theor. Biol.* 55:13–27.
21. Mathias, R. T., G. J. Baldo, K. Manivannan, and S. McLaughlin. 1991. Discrete charges on biological membranes. *In* Electrified Interfaces in Physics, Chemistry and Biology. R. Guidelli, editor. Kluwer Academic Publishers, Dordrecht, The Netherlands.
22. Sauvé, R., and S. Ohki. 1979. Interactions of divalent cations with negatively charged membrane surfaces. 1. Discrete charge potential. *J. Theor. Biol.* 81:157–179.
23. Loeb, A. 1951. An interionic attraction theory applied to the diffuse layer around colloid particles. *J. Colloid Sci.* 6:75–91.
24. Levine, S., K. Robinson, G. M. Bell, and J. Mingins. 1972. The discreteness-of-charge effect at charged aqueous interfaces. *J. Electroanal. Chem.* 38:253–269.
25. Duniec, J. T., and S. W. Thorne. 1981. Effects of discrete charges and dielectric properties of membrane–water interface on electric potentials inside membranes. *FEBS (Fed. Eur. Biochem. Soc.) Lett.* 126:1–4.
26. Duniec, J. T., and S. W. Thorne. 1983. Electrostatic potentials in membrane systems. *Bull. Math. Biol.* 45:69–90.
27. Fernández, M. S., and P. Fromherz. 1977. Lipoid pH indicators as probes of electrical potential and polarity in micelles. *J. Phys. Chem.* 81:1755–1761.
28. Cevc, G., A. Watts, and D. Marsh. 1981. Titration of the phase transition of phosphatidylserine bilayer membranes. Effects of pH, surface electrostatics, ion binding, and head-group hydration. *Biochemistry.* 20:4955–4965.
29. McLaughlin, S., N. Mulrine, T. Gresalfi, G. Vaio, and A. McLaughlin. 1981. Adsorption of divalent cations to bilayer membranes containing phosphatidylserine. *J. Gen. Physiol.* 77:445–473.
30. Henderson, D. 1986. Recent developments in the theory of electrified interfaces. *In* Trends in Interfacial Electrochemistry. A. F. Silva, editor. Reidel, Boston. 473–521.
31. Cevc, G. 1990. Membrane electrostatics. *Biochim. Biophys. Acta.* 1031:311–382.
32. Torrie, G. M., and J. P. Valleau. 1982. Electical Double Layers. 4. Limitation of the Gouy–Chapman Theory. *J. Phys. Chem.* 86:3251–3257.
33. Torrie, G. M. 1980. Electrical double layers. 1. Monte Carlo study of a uniformly charged surface. *J. Chem. Phys.* 73:5807–5816.
34. Torrie, G. M., and J. P. Valleau. 1979. A Monte Carlo study of an electrical double layer. *Chem. Phys. Lett.* 65:343–346.
35. Jackson, J. D. 1975. Classical Electrodynamics. John Wiley & Sons, Inc., New York. Chapter 1.
36. Kawasaki, K. 1972. Kinetics of Ising models. *In* Phase Transitions and Critical Phenomena. C. Domb and M. S. Green, editors. Academic Press, London. 443–501.
37. Jan, N., T. Lookman, and D. A. Pink. 1984. On computer simulation methods used to study models of two-component lipid bilayers. *Biochemistry.* 23:3227–3231.
38. Haile, J. M. 1986. On the use of computer simulation to determine the excess free energy in fluid mixtures. *Fluid Phase Equilibria.* 26:103–127.
39. Kirkwood, J. G. 1935. Statistical mechanics of fluid mixtures. *J. Chem. Phys.* 3:300–313.
40. Kirkwood, J. G. 1936. Statistical mechanics of liquid solutions. *Chem. Rev.* 19:275–307.
41. Shing, K. S., and K. E. Gubbins. 1983. A review of methods for predicting fluid phase equilibria: theory and computer simulation. *In* Advances in Chemistry Series. Vol. 204. J. M. Haile and G. A. Mansoori, editors. American Chemical Society, Washington, DC. 73–106.
42. Rovere, M., D. W. Heermann, and K. Binder. 1990. The gas–liquid transition of the two-dimensional Lennard-Jones fluid. *J. Phys.: Condens. Matter.* 2:7009–7032.
43. Levine, B., J. Mingins, and G. M. Bell. 1963. The discrete-ion effect and surface potentials of ionized monolayers. *J. Phys. Chem.* 67:2095–2105.
44. Levine, S., J. Mingins, and G. M. Bell. 1965. The diffuse layer correction to the discrete-ion effect in electric double layer theory. *Can. J. Chem.* 43:2834–2866.
45. Nir, S., C. Newton, and D. Papahadjopoulos. 1978. Binding of cations to phosphatidylserine vesicles. *Bioelectrochem. Bioenerg.* 5:116–133.
46. Eisenberg, M., T. Gresalfi, T. Riccio, and S. McLaughlin. 1979. Adsorption of monovalent cations to bilayer membranes containing negative phospholipids. *Biochemistry.* 18:5213–5223.
47. Träuble, H., and E. Sackmann. 1972. Studies of the crystalline-liquid crystalline phase transition of lipid model membranes. III. Structure of a steroid–lecithin system below and above the lipid-phase transition. *J. Am. Chem. Soc.* 94:4499–4510.
48. McLaughlin, A. C. 1982. Phosphorus-31 and carbon-13 nuclear magnetic resonance studies of divalent cation binding to phosphatidylserine membranes: Use of cobalt as a paramagnetic probe. *Biochemistry.* 21:4879–4885.